Interannual Variability in the Large-Scale Dynamics of the South Asian Summer Monsoon

JENNIFER M. WALKER, SIMONA BORDONI, AND TAPIO SCHNEIDER*

California Institute of Technology, Pasadena, California

(Manuscript received 2 September 2014, in final form 24 December 2014)

ABSTRACT

This study identifies coherent and robust large-scale atmospheric patterns of interannual variability of the South Asian summer monsoon (SASM) in observational data. A decomposition of the water vapor budget into dynamic and thermodynamic components shows that interannual variability of SASM net precipitation ($P - E$) is primarily caused by variations in winds rather than in moisture. Linear regression analyses reveal that strong monsoons are distinguished from weak monsoons by a northward expansion of the cross-equatorial monsoonal circulation, with increased precipitation in the ascending branch. Interestingly, and in disagreement with the view of monsoons as large-scale sea-breeze circulations, strong monsoons are associated with a decreased meridional gradient in the near-surface atmospheric temperature in the SASM region. Teleconnections exist from the SASM region to the Southern Hemisphere, whose midlatitude poleward eddy energy flux correlates with monsoon strength. Possible implications of these teleconnection patterns for understanding SASM interannual variability are discussed.

1. Introduction

The South Asian summer monsoon (SASM) displays variability on time scales from intraseasonal, through interannual, to decadal and beyond (e.g., Webster et al. 1998; Gadgil 2003; Turner and Annamalai 2012; Schneider et al. 2014). The standard deviation of interannual variability of SASM rainfall amounts to approximately 10% of the long-term mean summer rainfall (Gadgil 2003). This year-to-year variability of the SASM is sufficient to trigger drought and flood conditions, with major agricultural, economic, and social impacts (e.g., Gadgil and Kumar 2006).

Despite having been studied for many decades, the interannual variability of the SASM remains poorly understood and predicted. Many factors that influence variations of the SASM precipitation on interannual time scales have been investigated. Some studies have focused on the influence of sea surface temperatures (SSTs), particularly El Niño–Southern Oscillation (ENSO; e.g., Pant and Parthasarathy 1981; Rasmusson and Carpenter 1982; Meehl 1987; Webster and Yang 1992) and the east–west Indian Ocean dipole (IOD; e.g., Cherchi and Navarra 2013). Others have focused on land processes such as snow cover on the Tibetan Plateau and in Eurasia (e.g., Blanford 1884; Hahn and Shukla 1976; Meehl 1994; Shuen et al. 1998; Wu and Kirtman 2003). Of these factors, the strongest association has been found with ENSO. However, ENSO variations account for less than half of the total variation in SASM precipitation (Webster et al. 1998), and the relationship appears to have weakened in recent decades (Kumar et al. 1999, 2006).

In this study, we investigate the interannual variability of the SASM using observational data. Although there is considerable regional variability within the SASM domain, we first address the year-to-year variations of the large-scale monsoonal circulation, rather than local or regional features, and we primarily focus on large-scale atmospheric budgets such as the moisture, energy, and momentum budgets. Our approach is motivated by recent advances in the fundamental theoretical understanding of large-scale monsoonal circulations, such as the SASM.

Traditionally, the SASM has been viewed as a large-scale sea-breeze circulation, driven by surface temperature contrasts and their associated atmospheric pressure gradients between the Asian continent to the north and the Indian Ocean to the south (e.g., Webster

* Current affiliation: Department of Earth Sciences, ETH Zurich, Zurich, Switerland.

Corresponding author address: Jennifer M. Walker, California Institute of Technology, 1200 E. California Blvd., Pasadena, CA 91125.
E-mail: jwalker@caltech.edu

DOI: 10.1175/JCLI-D-14-00612.1

© 2015 American Meteorological Society

and Fasullo 2003). The sea-breeze paradigm has been extended to include the effects of elevated diabatic heating from moist convection (e.g., Webster et al. 1998) and the Tibetan Plateau (e.g., Li and Yanai 1996), consistent with recent observational studies that have shown that interannual variability of the SASM circulation is more strongly correlated with upper-tropospheric thermal contrasts than lower-tropospheric thermal contrasts (Sun et al. 2010; Dai et al. 2013). Whether the emphasis is on surface thermal contrasts or upper-tropospheric thermal contrasts, however, these studies take the surface inhomogeneities between land and ocean as an essential mechanism driving the SASM circulation; they view the meridional temperature gradient as a driver of monsoon circulations that can, to some extent, be considered as controlled by factors external to the monsoon circulations.

In recent years, an alternative theoretical framework has emerged, which views the SASM as the regional manifestation of the seasonal migration of the intertropical convergence zone (ITCZ) (e.g., Chao 2000; Chao and Chen 2001; Gadgil 2003). The monsoonal convergence is the root of the ascending branch of a thermally direct monsoonal overturning circulation, which shapes meridional temperature gradients and approaches conservation of angular momentum in its upper branch (e.g., Privé and Plumb 2007; Schneider and Bordoni 2008; Bordoni and Schneider 2008). In support of this view, modeling studies have shown that monsoonal circulations can exist even on aquaplanets without any land–ocean thermal contrasts (Privé and Plumb 2007; Bordoni and Schneider 2008), provided that the lower boundary has a small enough thermal inertia to allow for the ITCZ to migrate poleward into the subtropics. In this framework, the meridional temperature gradient (e.g., Li and Yanai 1996) and convective heating (e.g., Gill 1980) are viewed as being primarily controlled by the monsoon circulation, forming the atmosphere's response to the seasonal variation of insolation. Consistent with quasi-equilibrium (QE) theories of moist convection (e.g., Emanuel et al. 1994), latent heat release is posited to relax the atmosphere to a convectively neutral stratification, rather than to act as a driver for the monsoonal circulation (e.g., Privé and Plumb 2007). Observational studies have confirmed that the free-tropospheric temperature in the ascending branch of the SASM circulation is coupled to the subcloud equivalent potential temperature, a finding consistent with the assumption of convective quasi-equilibrium (Nie et al. 2010; Hurley and Boos 2013).

To the extent that monsoonal circulations form an essential part of the seasonal Hadley circulation, analyses of large-scale budgets zonally averaged over wide longitude sectors can prove useful in investigating how SASM interannual variability arises. For instance, Schneider and Bordoni (2008) and Bordoni and Schneider (2008) suggest that the onset of the SASM might be interpreted as a shift of the dominant balance in the upper-tropospheric zonal momentum budget, from a budget dominated by eddy momentum fluxes to one dominated by momentum transport by the cross-equatorial Hadley cell. Other studies have analyzed how extratropical thermal forcings, such as changes in glaciation or in the strength of the Atlantic meridional overturning circulation, can influence the location of the zonally and annually averaged ITCZ, through shifts toward a differentially warming hemisphere (e.g., Chiang and Bitz 2005; Kang et al. 2008; Chiang and Friedman 2012; Bischoff and Schneider 2014). These studies have emphasized the role of the cross-equatorial energy transport and the atmospheric energy budget in controlling the position of the tropical precipitation, through mechanisms that might also be relevant to the SASM (Schneider et al. 2014).

Here we investigate SASM interannual variability observationally, beginning by developing a new index for the SASM strength that links monsoon precipitation to the large-scale circulation more directly than existing indices. We examine correlations between the SASM strength and large-scale dynamics both within the monsoon region and globally, to explore possible local and nonlocal influences on the monsoon. Using reanalysis and precipitation data, we seek to answer the following questions:

1) Is the interannual variability in SASM precipitation dominated by changes in the circulation or by changes in atmospheric moisture?
2) What large-scale dynamic and thermodynamic patterns are associated with strong and weak monsoon years?
3) Are there connections between extratropical eddy activity and SASM interannual variability?

To address question 1, we decompose the atmospheric moisture budget of the SASM into dynamic and thermodynamic components, and we use linear regression analyses to address questions 2 and 3. Section 2 describes the data sources and methods used in our analysis. In section 3, we examine the atmospheric moisture budget of the SASM and introduce the new monsoon index. In section 4, we evaluate dynamic and thermodynamic patterns associated with strong and weak monsoon years. In section 5, we explore teleconnections between the SASM and the extratropics, especially in the Southern Hemisphere. In section 6, we discuss the possible influence of ENSO and IOD on the results

presented in sections 4 and 5. We summarize our findings and provide concluding remarks in section 7.

2. Data and methods

Winds, atmospheric temperature, and specific humidity for the years 1979–2011 are used from the 6-hourly data of the European Centre for Medium-Range Weather Forecasts (ECMWF) interim reanalysis (ERA-Interim; Dee et al. 2011), on 60 vertical levels on terrain-following coordinates up to 0.1 hPa and with spectral T255 horizontal resolution (grid resolution approximately $0.7° \times 0.7°$). Precipitation data are from the Global Precipitation Climatology Project (GPCP; Adler et al. 2003) version 2.2, a set of gridded monthly precipitation estimates based on satellite and rain gauge data, at $2.5° \times 2.5°$ horizontal resolution. To determine which findings are robust across datasets, we compare our results with the following additional reanalysis products: National Centers for Environmental Prediction (NCEP)–National Center for Atmospheric Research (NCAR) Reanalysis 1 (NCEP1; Kalnay et al. 1996), NCEP–U.S. Department of Energy (DOE) Reanalysis 2 (NCEP2; Kanamitsu et al. 2002), 40-yr ECMWF Re-Analysis (ERA-40; Uppala et al. 2005), and the Twentieth Century Reanalysis Project version 2 from the National Oceanic and Atmospheric Administration (NOAA) and the Cooperative Institute for Research in Environmental Sciences (CIRES) at the University of Colorado (20CENTURY) (Compo et al. 2011). The findings presented here are robust across all of these reanalysis products except where otherwise noted.

To examine the interannual variations of the SASM, we focus on the warm season months from June to September (JJAS), and we introduce a novel yearly monsoon index based on the large-scale moisture budget. The methodology used to develop this monsoon index is described in detail in section 3; in essence, our index is based on ERA-Interim JJAS averaged moisture flux convergence over a region representative of the large-scale SASM circulation (10°–30°N, 60°–100°E). This region is similar to SASM regions used in previous studies (Goswami et al. 1999; Wang and Fan 1999; Hurley and Boos 2013); it was chosen to include the climatological precipitation maxima over India and the Bay of Bengal. The results shown here are robust to different choices of averaging regions, as long as the averaging region does not extend in longitude too far east into Southeast Asia, where the interannual precipitation variability is anticorrelated with that of the Indian monsoon, as will be discussed in section 4.

Large-scale dynamics and precipitation patterns associated with strong and weak SASM years are investigated by performing linear regression analyses using the monsoon strength index, standardized by its standard deviation, and the atmospheric and precipitation fields from ERA-Interim and GPCP, respectively. For each data field considered (e.g., wind, temperature, and precipitation), the linear regression is calculated at each data point by regressing the 1979–2011 time series of yearly JJAS averaged values of the data field at that point, against the monsoon index. Focus is on the interannual variability; the long-term linear trend from 1979–2011 is removed from the monsoon index and from the data fields in the regression analysis. However, in the appendix we provide a brief discussion of trends inferred from the ERA-Interim and other reanalysis products, and compare those with trends recently highlighted in the literature (e.g., Bollasina et al. 2011; Zuo et al. 2013).

Statistical significance of the correlation coefficient at each point is computed by a Student's t test, and correlations that are statistically significant at the 5% level are highlighted. Composite analysis of the five strongest and five weakest monsoon years shows similar results to the linear regression analysis.

Given that interannual variability in SSTs of surrounding ocean basins has been shown to influence the SASM interannual variability in many previous studies, we also explore if and to what extent patterns exposed here are associated with ENSO and IOD variability.

As an ENSO index, we use the June–August (JJA) average Niño-3.4 index (Trenberth 1997a) from NOAA. Anomalous ENSO signals tend to be maximal during the boreal winter months December–February (DJF); the JJA average value of Niño-3.4 is strongly correlated with its average value in the following DJF, and thus the JJA Niño-3.4 represents El Niño/La Niña conditions that are developing during the summer monsoon season and the following winter.

The IOD is a measure of the SST gradient between the western equatorial Indian Ocean and the southeastern equatorial Indian Ocean (Saji et al. 1999). As an index for the IOD, we use the JJA average dipole mode index (DMI) derived from the Hadley Centre Sea Ice and Sea Surface Temperature dataset (HadISST), provided by the Japan Agency for Marine-Earth Science and Technology (http://www.jamstec.go.jp/frsgc/research/d1/iod/e/iod/dipole_mode_index.html).

Transient eddy fields are computed for each month of each year by subtracting the monthly mean field from that year and by taking an average, weighted by the number of days per month, of the monthly eddy fields for the seasonal average. Horizontal eddy momentum flux divergence is computed as $\nabla \cdot (\overline{u'\mathbf{u}'}\cos\phi)$, where $\mathbf{u} = (u, v)$ is the horizontal velocity field, ϕ is latitude, and primes denote transient eddy fields.

3. Atmospheric moisture budget

a. *Dynamic and thermodynamic components of interannual variability*

In a long-term mean, when changes in atmospheric moisture content can be neglected, the vertically integrated moisture budget relates the net precipitation ($P - E$) to the convergence of the water vapor flux, that is

$$\overline{P} - \overline{E} = \mathrm{MFC} = -\int_0^{p_s} \nabla_p \cdot (\overline{\mathbf{u}}\overline{q})\frac{dp}{g}, \qquad (1)$$

where MFC is the vertically integrated horizontal moisture flux convergence, $\nabla_p \cdot (\,)$ is the horizontal divergence in pressure coordinates, $\mathbf{u} = (u, v)$ is the horizontal wind vector, q is the specific humidity, P is the precipitation rate, and E is the evaporation rate (Peixoto and Oort 1992). Overbars denote the time mean, in our case over a season.

We study the large-scale SASM moisture budget by averaging the vertically integrated horizontal moisture flux convergence from Eq. (1) over the region 10°–30°N, 60°–100°E (shown in Fig. 3) using the ERA-Interim winds and specific humidity averaged over JJAS of each year. This formulation allows us to decompose the monsoon net precipitation into dynamic and thermodynamic components, similar to decompositions performed in previous studies for the zonally averaged circulation (e.g., Held and Soden 2006), for the response of monsoons to orbital precession (Clement et al. 2004; Merlis et al. 2013), and for the response of monsoons to anthropogenic forcings (Hsu et al. 2013). Specifically, we decompose the yearly JJAS horizontal moisture fluxes $\mathbf{u}q$ according to

$$\delta(\mathbf{u}q) = \overline{\mathbf{u}}\delta q + \overline{q}\delta\mathbf{u} + \delta\mathbf{u}\delta q, \qquad (2)$$

where δ represents the year-to-year deviation from the climatological mean. In Eq. (2), the first term on the right-hand side represents the thermodynamic component, in which the winds are fixed at their climatological value, and the atmospheric moisture varies from year to year; the second term represents the dynamic component, in which the atmospheric moisture is fixed at its climatological value, and the winds vary from year to year; and the third term is the quadratic term, which we found to be negligible in the SASM moisture budget.

Figure 1 shows that the interannual variability in SASM net precipitation in ERA-Interim is dominated by the dynamic component, which accounts for 92% of the interannual variability, while the thermodynamic component accounts for only 8%. Decomposition of the dynamic term into zonal and meridional components shows that both components contribute significantly to the total variability; the zonal component dominates slightly, with correlation coefficients of 0.62 and 0.38 between the dynamic term of MFC and its zonal and meridional components, respectively. The dominance of the dynamic term is robust across all reanalysis datasets, with the year-to-year variations in SASM net precipitation strongly dominated by variations in the monsoon winds and circulation, rather than variations in atmospheric moisture. This emphasizes the importance of understanding interannual patterns in the SASM large-scale circulation to understand the interannual variability of the SASM precipitation.

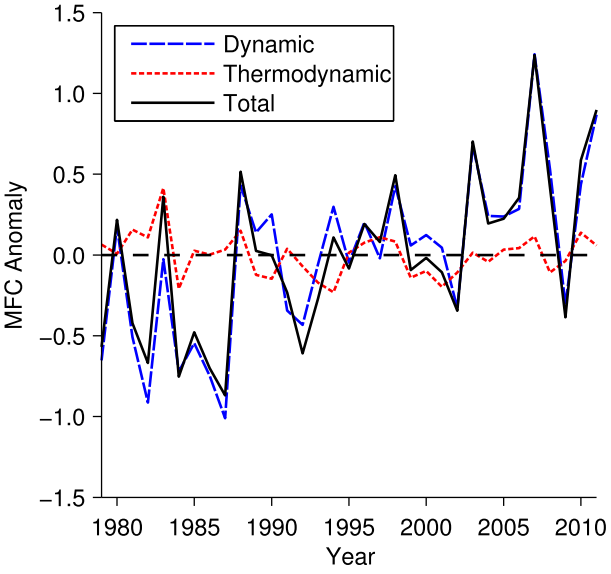

FIG. 1. Interannual variability of the SASM strength based on the ERA-Interim atmospheric moisture budget, showing the dynamic component, thermodynamic component, and total variability (mm day^{-1}).

b. *Large-scale monsoon index*

The choice of an index to characterize the interannual variability of the SASM has been studied extensively in recent decades. There is no consensus on a single index as the best measure of SASM strength, and many different approaches have been used.

The all India rainfall (AIR) index is an area-weighted average of rainfall measured at rain gauge stations distributed over India (Parthasarathy et al. 1992, 1995). It has been used by the Indian Meteorological Department in many studies of SASM interannual variability and prediction (e.g., Shukla and Mooley 1987; Meehl 1987; Yasunari 1991). While it is a particularly relevant monsoon index from a socioeconomic perspective, the AIR may not fully represent the large-scale monsoonal circulation, since it is limited

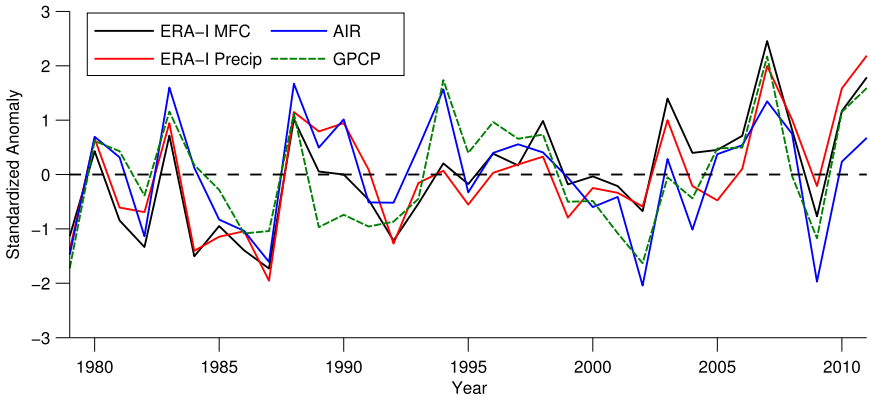

FIG. 2. Time series of the MFC index, based on ERA-Interim atmospheric moisture budget, along with precipitation from ERA-Interim and GPCP averaged over the same region (10°–30°N, 60°–100°E), and the AIR index. Each time series is based on JJAS averages, and is shown as the standardized anomaly from the climatological mean.

to the Indian subcontinent and does not include neighboring land and ocean areas with significant monsoon precipitation (cf. Goswami et al. 1999).

Webster and Yang (1992) introduced a dynamically based monsoon index, in which the large-scale monsoonal circulation is interpreted as a Rossby wave response to midtropospheric latent heat released by monsoon convection over South Asia. The dynamic response is dominated by the lowest baroclinic mode and exhibits vertical wind shear related to the strength of the heat source, and thus to the monsoon precipitation (Webster 1972; Gill 1980). Webster and Yang (1992) defined their monsoon index (hereafter WYI) as the zonal wind shear between 850 and 200 hPa, U850 − U200, averaged over the region 0°–20°N, 40°–110°E. Through thermal wind balance, WYI links the zonal wind shear to the meridional temperature gradient and hence to the land–sea thermal contrast. This index, by construction, captures well the SASM in terms of the zonal wind shear; it also captures the strength of the low-level westerly jet and upper-level easterly jet in the NCEP–NCAR reanalysis (Wang and Fan 1999).

However, the weak correlation between the WYI and the AIR (Webster and Yang 1992), as well as significant influences of western Pacific convective activity on the WYI (Ailikun and Yasunari 1998; Wang and Fan 1999), has motivated the introduction of other dynamically based indices to represent the SASM. Other wind shear-based indices include the westerly shear averaged over a different region (Wang and Fan 1999) and the shear in meridional velocity (Goswami et al. 1999); these indices have been shown to correlate well with each other and with the WYI and AIR.

In the previous section, we showed that the vertically integrated moisture flux convergence averaged over the region 10°–30°N, 60°–100°E, an index we shall denote as MFC, is by construction related to the SASM net precipitation. Figure 2 shows MFC along with ERA-Interim and GPCP precipitation averaged over the same geographic region and along with the AIR index from the Indian Institute of Tropical Meteorology. MFC is highly correlated with these other measures of SASM precipitation, with correlation coefficients of 0.87, 0.75, and 0.80 between the detrended MFC and the detrended ERA-Interim precipitation, GPCP precipitation, and AIR, respectively. The correlation between the detrended MFC and WYI is weak (0.22) and not statistically significant at the 5% level, consistent with the weak correlation between WYI and AIR (Webster and Yang 1992).

Since the interannual variability in MFC is dominated by the dynamic component, MFC is a measure of both net precipitation intensity and of the strength of the large-scale SASM circulation. Therefore, we select MFC as an index for the SASM strength because it accounts for most of the interannual variability in both the precipitation and circulation of the SASM. Additionally, it is more robust than precipitation data alone because the moisture flux convergence is controlled by large-scale processes that are better constrained by data. Unlike other dynamical indices that are based on wind shear, under the assumption that temperature gradients are driving the monsoon circulation, MFC is a dynamical index that does not require any such assumptions about the driving mechanisms of the SASM.

On top of the strong interannual variability, the MFC index in Fig. 2 shows a slight increasing trend. This is in disagreement with trends in Indian precipitation highlighted by other studies (e.g., Ramanathan et al. 2005; Bollasina et al. 2011) and, as discussed in the appendix, is not robust across all datasets.

4. Large-scale patterns of monsoon variability

a. Precipitation and meridional overturning circulation

The MFC index of SASM interannual variability allows us to investigate large-scale dynamic and thermodynamic patterns associated with strong (weak) monsoon years. Figure 3 shows the climatology of GPCP precipitation over the SASM domain (Fig. 3a) and the local regression coefficients of the precipitation field onto the MFC index (Fig. 3b). A similar analysis using ERA-Interim data shows that the contribution of evaporation is negligible (not shown), so that the variability in total precipitation associated with strong (weak) monsoons is approximately equal to the variability in net precipitation. Over India and much of South Asia, there is a strong positive correlation between the measured precipitation and the MFC index. Over the eastern Bay of Bengal, which is a center of maximum SASM precipitation in the climatological mean, the interannual variability of precipitation is negatively correlated with the MFC index; precipitation over this region is lower during a strong SASM. This zonal asymmetry is robust across multiple precipitation datasets and different monsoon indices (not shown) and is consistent with Wang et al. (2001), who show that the two precipitation maxima over India and over the eastern Bay of Bengal have distinct interannual variations.

East of the SASM region, over the tropical Pacific Ocean, the regression analysis shows a strong negative correlation between precipitation and SASM strength north of the equator, and a strong positive correlation south of the equator (Fig. 3), indicating a southward shift of the ITCZ over the western tropical Pacific. While evident in ERA-Interim and partly explained by ENSO variability, this feature does not appear to be robust across all reanalysis datasets.

Figures 4a–c show the ERA-Interim JJAS climatology of the SASM meridional overturning circulation, as measured by the 60°–100°E sector mean (hereafter denoted as the SASM sector) Eulerian mass streamfunction (Fig. 4a), vertical pressure velocity (Fig. 4b), and meridional velocity (Fig. 4c). The climatological fields of meridional and vertical pressure velocity show northward flow from the Southern Hemisphere to the Northern Hemisphere in the lower troposphere, ascent in the Northern Hemisphere tropics and subtropics, southward cross-equatorial flow in the upper troposphere, and subsidence in the Southern Hemisphere tropics and subtropics. Together these winds form a thermally direct circulation that has the character of a broad, cross-equatorial Hadley cell, consistent with previous descriptions of the SASM (e.g., Webster et al. 1998; Trenberth et al. 2005). This circulation is illustrated in the climatological Eulerian mass streamfunction in Fig. 4a, with maximum streamfunction, and hence maximum meridional mass transport, near the equator. Within the SASM sector, the dominant mass balance is between the meridional and vertical fluxes, as expected, with zonal fluxes into or out of the sector contributing less than 30% of the mass budget. The maximum SASM precipitation is located in the latitudes of the ascending branch of this circulation (Figs. 3 and 6), where the ascending motion maximizes.

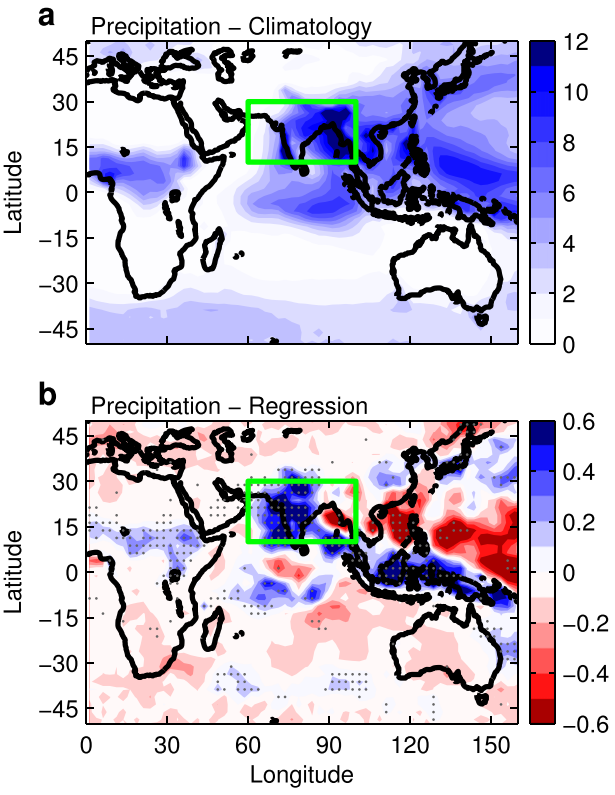

FIG. 3. JJAS precipitation (mm day^{-1}) from GPCP, showing (a) 1979–2011 climatology and (b) regression coefficients from linear regression of JJAS precipitation for each year against the standardized MFC index. Gray stippling in (b) shows regions where the regression coefficient is significant at the 5% level. The green rectangle shows the averaging region for the MFC index.

Linear regression of the streamfunction, vertical pressure velocity, and meridional velocity onto the MFC index (Figs. 4d–f) shows that strong monsoons are associated with a change in the structure of the meridional circulation with increased ascent farther north and a correspondingly northward extended circulation. To further highlight differences in the SASM overturning circulation between strong and weak monsoon years, in Fig. 5, we show "strong" ("weak") streamfunctions defined as the climatological streamfunction plus

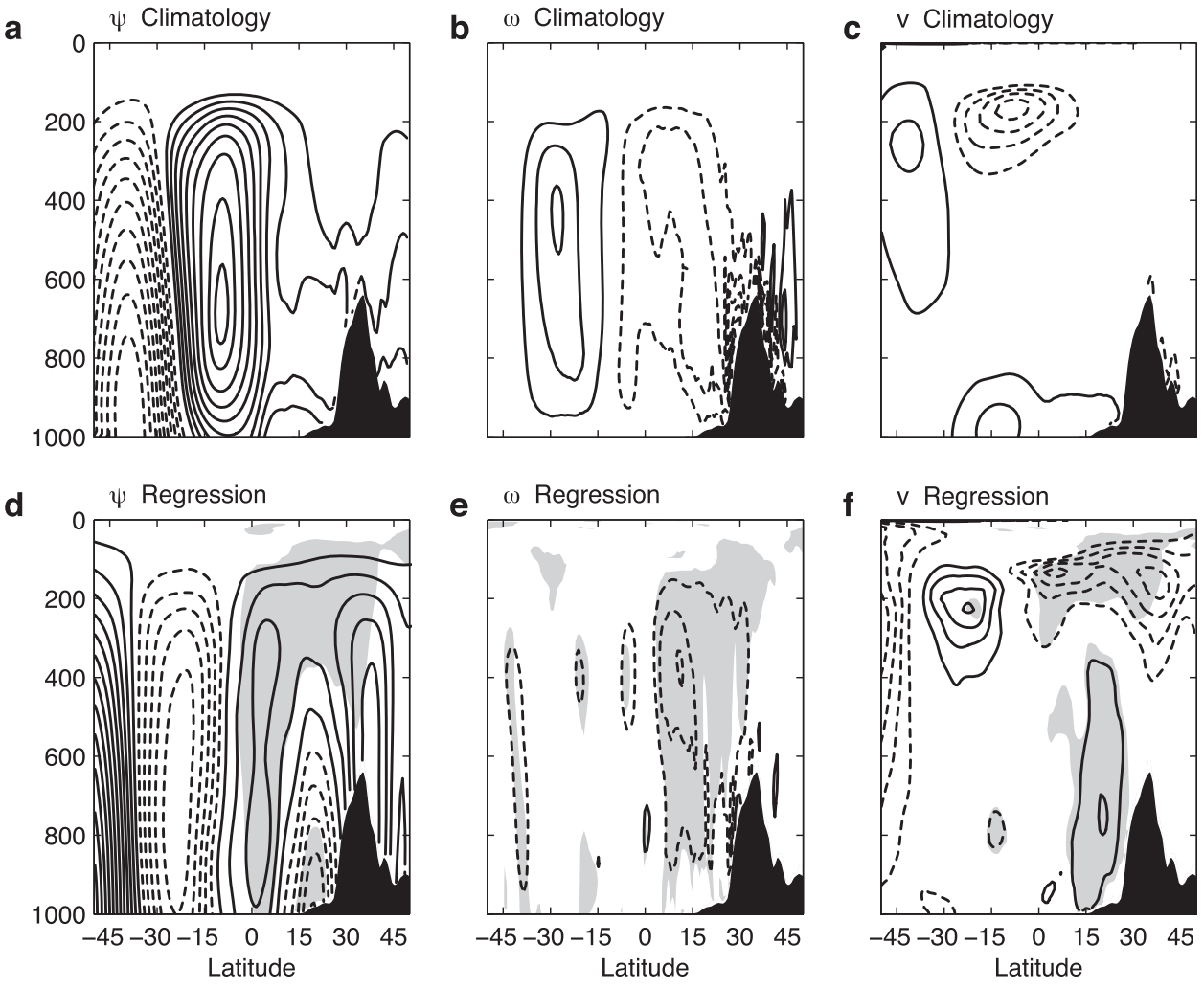

FIG. 4. (a)–(c) Climatology and (d)–(f) regression coefficients onto MFC index of JJAS ERA-Interim SASM sector (left)–(right) mean streamfunction, vertical pressure velocity, and meridional velocity. Solid contours are positive, while dashed contours are negative; zero contours are omitted. Gray shading in (d)–(f) shows regions where the regression coefficient is significant at the 5% level. Black shading shows the sector mean topography. Contour intervals are 5×10^9 kg s^{-1}, 0.02 Pa s^{-1}, 2 m s^{-1}, 0.5×10^9 kg s^{-1}, 0.002 Pa s^{-1}, and 0.1 m s^{-1} in (a)–(f), respectively.

(minus) the regression coefficient times 2 standard deviations of MFC. The northward expansion of the strong monsoon circulation compared to the weak monsoon is evident, with a statistically significant positive correlation coefficient of 0.46 between the latitude of maximum streamfunction and the MFC index; this corresponds to a northward shift of approximately 1.38° in the latitude of maximum streamfunction per standard deviation of the MFC index (i.e., a 5.5° shift between the ±2 standard deviations for strong/weak monsoons in Fig. 5). Similarly, there is a statistically significant increase in streamfunction values in the ascending branch of the circulation (Fig. 4d).

Using GPCP precipitation data to define strong or weak precipitation profiles as defined for the streamfunction, we see in Fig. 6 that in the SASM sector, strong monsoons are associated with a strengthening of the precipitation and a northward shift of approximately 5° in the latitude of maximum precipitation. However, this result is not robust across all datasets, so it remains uncertain whether strong monsoons are indeed associated with a northward shift of the local ITCZ within the SASM sector. However, the northward shift in the meridional overturning circulation is robust.

b. Zonal winds

Figure 7 shows the climatology of ERA-Interim zonal winds at 850 and 200 hPa, while Fig. 8 shows the SASM sector mean zonal winds. The main features of the monsoonal circulation are evident in the climatology,

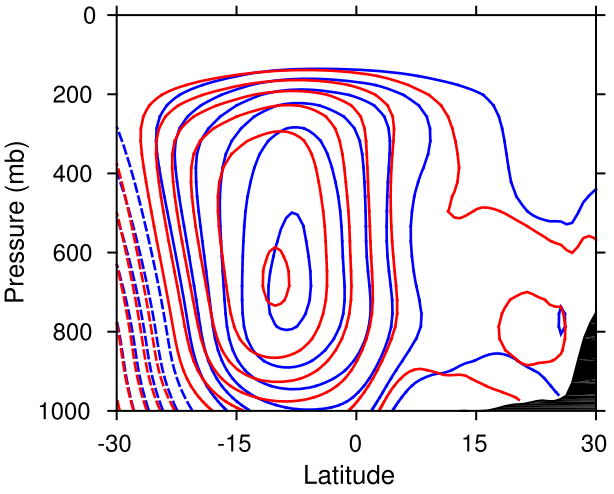

FIG. 5. Streamfunctions representing "strong" (blue) and "weak" (red) monsoonal circulations, defined as those associated with a ±2 standard deviation excursion of the MFC index. Positive contours are solid, negative contours are dashed, and zero contours are omitted. Contour interval is 5×10^9 kg s^{-1}.

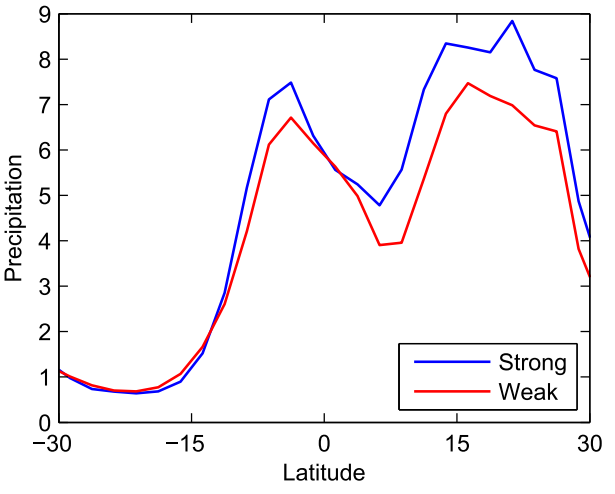

FIG. 6. SASM sector GPCP JJAS precipitation profiles (mm day^{-1}) for strong (blue) and weak (red) monsoons.

with an upper-level easterly jet in the tropics, a poleward displaced upper-level westerly jet, and lower-level westerly flow in the northern tropics over the Arabian Sea, Bay of Bengal, and Indian subcontinent. These features are also evident in a zonal average over the SASM sector (Fig. 8), which additionally reveals two distinct upper-level westerly jets in the Southern Hemisphere, with the subtropical jet centered near 30°S and the midlatitude jet centered near 45°S.

Linear regression onto the MFC index shows that strong monsoons are associated with a strengthened upper-level easterly jet in the tropics, enhanced lower-level westerly flow over the Arabian Sea, decreased lower-level westerly flow over the eastern Bay of Bengal, and increased lower-level easterly trade winds throughout the tropical Pacific Ocean (Fig. 7), consistent with previous findings (Webster and Yang 1992; Wang and Fan 1999). The zonally asymmetric lower-level zonal wind anomalies over the SASM region are consistent with the precipitation anomalies shown in Fig. 3b, with weakened zonal winds and weakened convergence over the eastern Bay of Bengal corresponding to weakened precipitation there in strong monsoons.

Figures 7 and 8 also reveal correlations between the MFC index and the zonal winds in the extratropics, with significant correlations in the Southern Hemisphere; these will be explored further in section 5.

c. *Atmospheric temperature*

In addition to the meridional overturning circulation and zonal winds, we look at atmospheric temperatures, particularly their meridional gradient, to seek patterns in upper- and lower-level temperatures associated with strong (weak) monsoons and to investigate the land–sea thermal contrast in the context of interannual variability. If the monsoon is largely driven by the land–sea thermal contrast, then we might expect that stronger monsoons would be accompanied by an increased near-surface thermal contrast, with higher than average temperatures over India and/or lower than average temperatures over the Indian Ocean. However, as far back as 1921, it was observed that average temperature in India is higher in summers with low monsoon rainfall than in summers with high monsoon rainfall (Simpson 1921).

Figure 9 shows the climatology of ERA-Interim atmospheric temperatures at 850 and 200 hPa. We see the reversal of the meridional temperature gradient at both levels, with temperature increasing poleward, and a strong maximum in upper-level temperature west of the Tibetan Plateau, consistent with previous studies (Molnar et al. 2010). Linear regression onto the MFC index shows that strong monsoons are associated with an increased meridional gradient in upper-tropospheric temperature in the monsoon region (Fig. 9c) (Li and Yanai 1996; Sun et al. 2010; Hurley and Boos 2013; Dai et al. 2013). We also see that strong monsoons are associated with positive anomalies in upper-level atmospheric temperature in the subtropics and extratropics of both hemispheres (Fig. 9c), consistent with a previous study (Hurley and Boos 2013). This symmetric pattern can be partially understood through axisymmetric theories of the circulation induced by off-equatorial heating (Lindzen and Hou 1988), which argue that for angular momentum conserving cross-equatorial circulations,

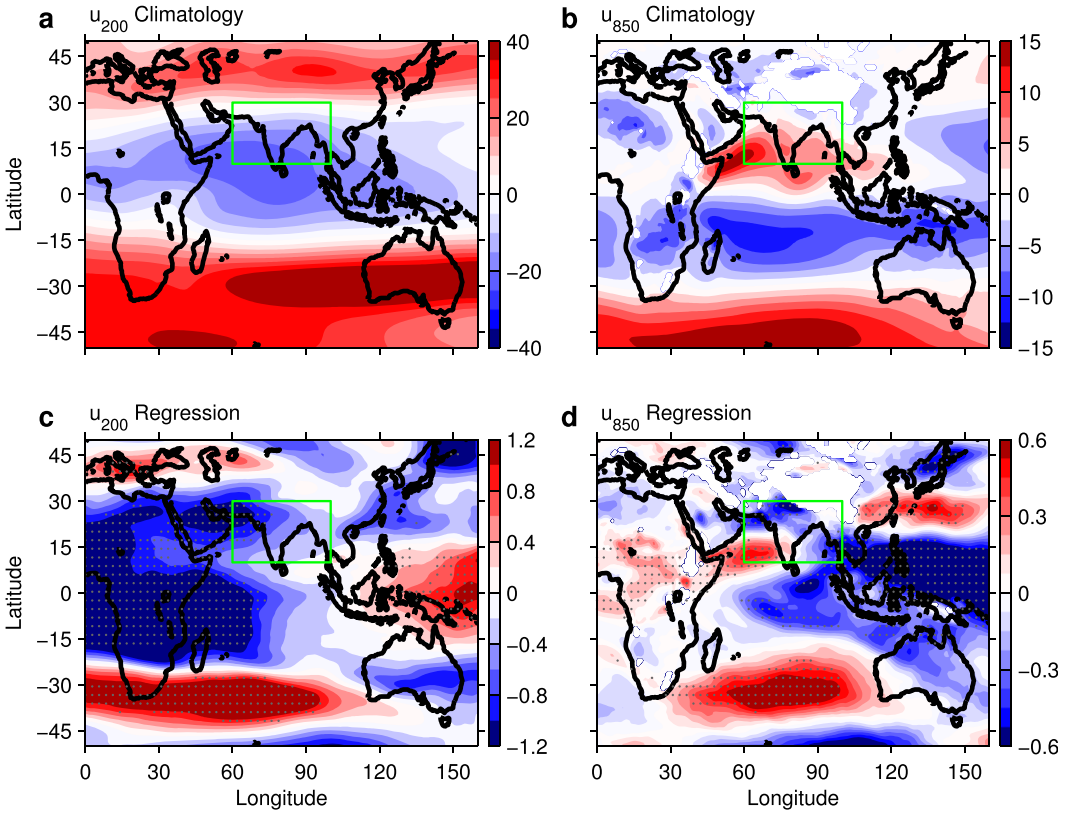

FIG. 7. (a),(b) Climatology and (c),(d) regression coefficient onto MFC index of JJAS ERA-Interim zonal wind ($m\,s^{-1}$) at (left) 200 and (right) 850 hPa. Gray stippling in (c),(d) shows the regions where the regression coefficient is significant at the 5% level. The green rectangle shows the averaging region for the MFC index.

free-tropospheric temperatures are symmetric about the equator, with an equatorial minimum and subtropical maxima in each hemisphere. For a circulation with ascending branch farther poleward, the subtropical maxima likewise shift poleward, along with the equatorial minimum becoming more pronounced. While similar changes are seen in subtropical temperatures (Fig. 9c), a deepening of the equatorial temperature minimum is not evident.

Figure 9 shows that strong monsoons are correlated with negative anomalies in near-surface temperature over India and a reduced meridional gradient in near-surface temperature between India and the ocean to the south. When the 850-hPa atmospheric temperature is averaged over land only (T_{land}) and over ocean only (T_{ocean}) over the region 10°S–30°N, 60°–100°E, we find that the near-surface land–ocean thermal contrast $dT = T_{land} - T_{ocean}$ is negatively correlated with the monsoon strength index, with a statistically significant correlation coefficient of −0.46.

These results are consistent with a similar linear regression involving subcloud atmospheric temperatures in a previous study (Hurley and Boos 2013), but they are inconsistent with other studies (Sun et al. 2010; Dai et al. 2013), which found a positive correlation between monsoon strength and lower-tropospheric thermal contrast (although this correlation was much weaker than the correlation with upper-level thermal contrast). A possible reason for this discrepancy is the choice of monsoon index. Sun et al. (2010) and Dai et al. (2013) use the shear-based Webster–Yang index for monsoon strength, which by construction is more strongly correlated with the meridional temperature gradient; however, it correlates less strongly with measures of monsoon precipitation and circulation strength.

One might posit that the near-surface thermal contrast could be higher than average in the spring and early stages of a strong summer monsoon, driving a stronger circulation. Once the monsoon has matured, the increased rainfall and soil moisture cool the lower troposphere over the Indian subcontinent, resulting in a negative correlation in the overall JJAS average. To investigate this possibility, we regressed the preceding spring March–May (MAM) averaged atmospheric

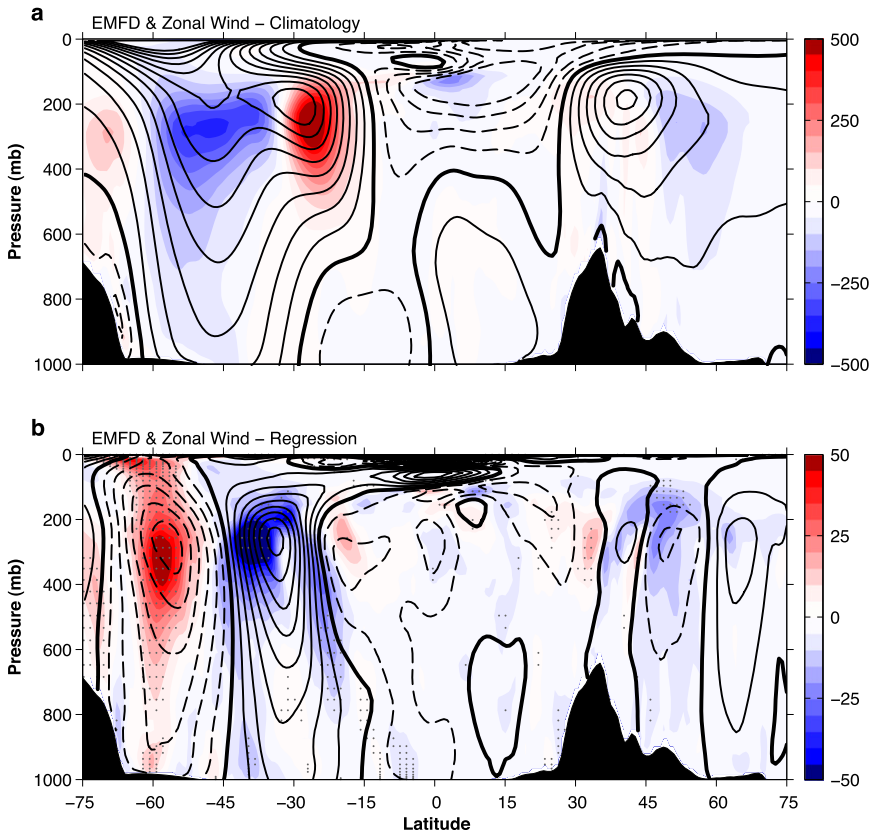

FIG. 8. (a) Climatology and (b) regression coefficient onto MFC index of JJAS ERA-Interim SASM sector EMFD (colors, $\mathrm{m\,s^{-2}}$) and zonal wind (contours, $\mathrm{m\,s^{-1}}$). Positive contours are solid, negative contours are dashed, and zero contours are thick solid. Gray stippling in (b) shows the regions where the EMFD regression coefficient is significant at the 5% level. Black shading shows the sector mean topography. Contour levels of zonal wind are 5 and 0.25 $\mathrm{m\,s^{-1}}$ in (a),(b), respectively.

temperatures onto the JJAS summer monsoon index and found that a reduced meridional gradient in near-surface temperature is also present in the spring preceding a strong monsoon, as illustrated in the strong and weak temperature profiles in Fig. 10. Comparing all reanalysis datasets, we do not find any robust indication of an increased near-surface thermal contrast in the spring preceding a strong monsoon, whereas we do find a robust decreased near-surface thermal contrast during the JJAS monsoon season. These results suggest that the near-surface temperature gradient should not be considered as an external forcing for the monsoon, but is itself a response to the atmospheric circulation, with stronger monsoonal circulations and increased monsoon rainfall smoothing the thermal gradient.

The regression of near-surface atmospheric temperatures onto the MFC index also shows statistically significant correlations in the Southern Hemisphere extratropics, with strong monsoons correlated with a negative anomaly in near-surface temperature from approximately 30° to 50°S, throughout the SASM longitudes and to the west (Fig. 9). The center of the cooling anomaly and the boundary between cooling and warming anomalies vary in longitude between reanalysis datasets, with these features shifted west in some datasets compared to ERA-Interim; however, the presence of a cooling anomaly over the extratropical southern Indian Ocean is a robust feature across all reanalysis products. This teleconnection pattern will be explored further in section 5.

To investigate the possible role of convective quasi-equilibrium in the SASM circulation, we also looked at subcloud equivalent potential temperatures (θ_{eb}) in the five reanalysis datasets (not shown). Consistent with quasi-equilibrium and previous observational studies (Nie et al. 2010; Hurley and Boos 2013), we find that the latitude of maximum θ_{eb} coincides with the latitude of maximum upper-level temperature in the climatology. Performing a linear regression analysis of θ_{eb} onto the MFC index, we find that strong monsoons are associated

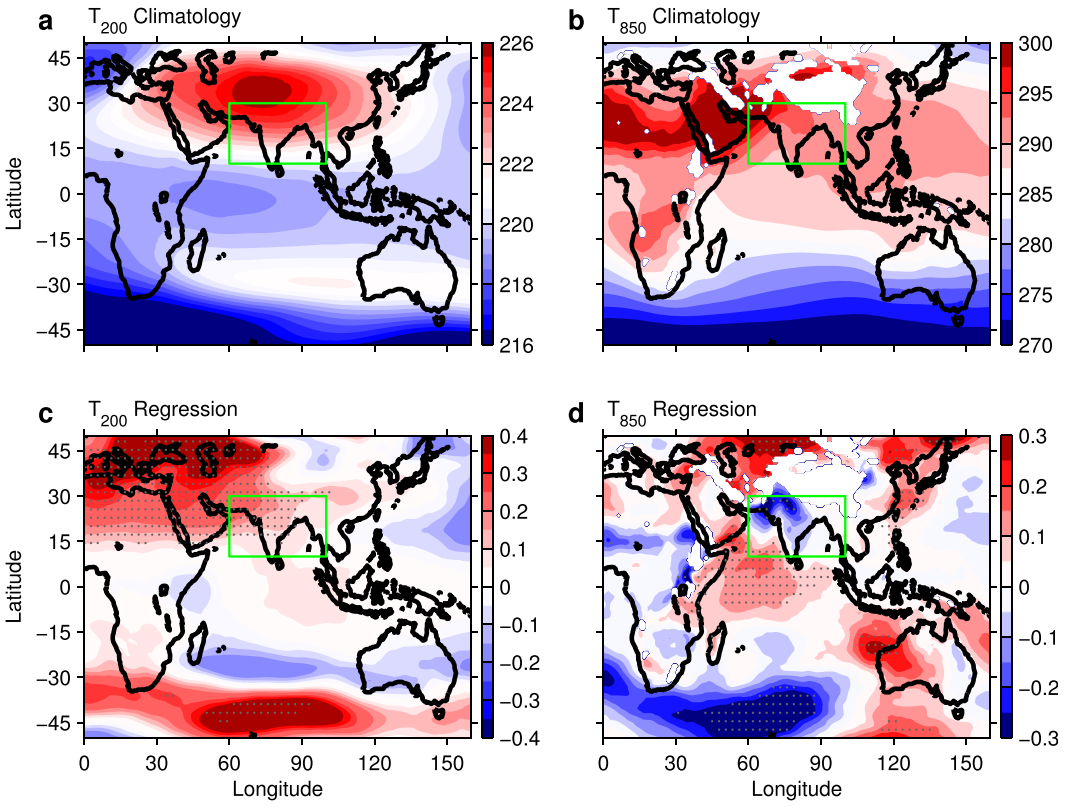

FIG. 9. (a),(b) Climatology and (c),(d) regression coefficient onto MFC index of JJAS ERA-Interim atmospheric temperature (K) at 200 and 850 hPa. Gray stippling in (c),(d) shows the regions where the regression coefficient is significant at the 5% level. The green rectangle shows the averaging region for the MFC index.

with an increased meridional gradient in JJAS subcloud equivalent potential temperature (θ_{eb}) across the SASM region, while the latitude of maximum θ_{eb} is the same for strong and weak monsoons, in agreement with previous findings (Hurley and Boos 2013).

5. Teleconnections with Southern Hemisphere extratropics

The northward shift of the monsoonal circulation during strong monsoon years (Fig. 4), along with the lower near-surface air temperature over the extratropical southern Indian Ocean (Fig. 9), is suggestive of a possible link between the monsoonal circulation and extratropical Southern Hemisphere thermal forcing. Recent model studies (e.g., Chiang and Bitz 2005; Broccoli et al. 2006; Kang et al. 2008; Chiang and Friedman 2012; Frierson and Hwang 2012; Bischoff and Schneider 2014; Schneider et al. 2014) have shown that thermal forcing in the extratropics can induce a shift in the zonally averaged ITCZ toward a differentially warming hemisphere: The extratropical thermal forcing is communicated by anomalous midlatitude eddy energy export out of the tropics, and the Hadley circulation responds with an anomalous cross-equatorial component. The anomalous Hadley circulation causes an

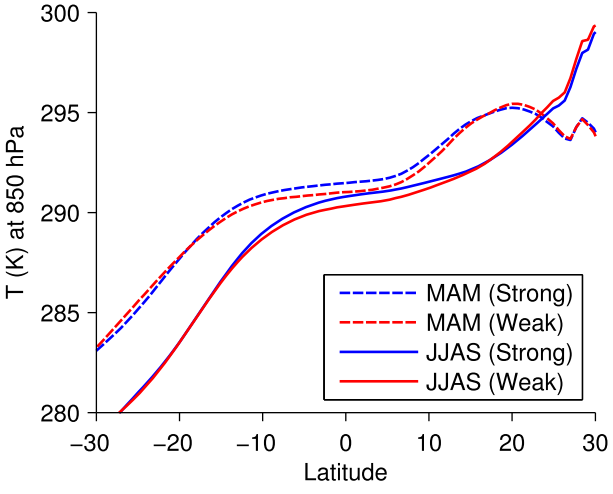

FIG. 10. SASM sector lower-tropospheric temperature (K) in MAM (dashed) and JJAS (solid) for strong (blue) and weak (red) monsoons, using ERA-Interim temperatures at 850 hPa.

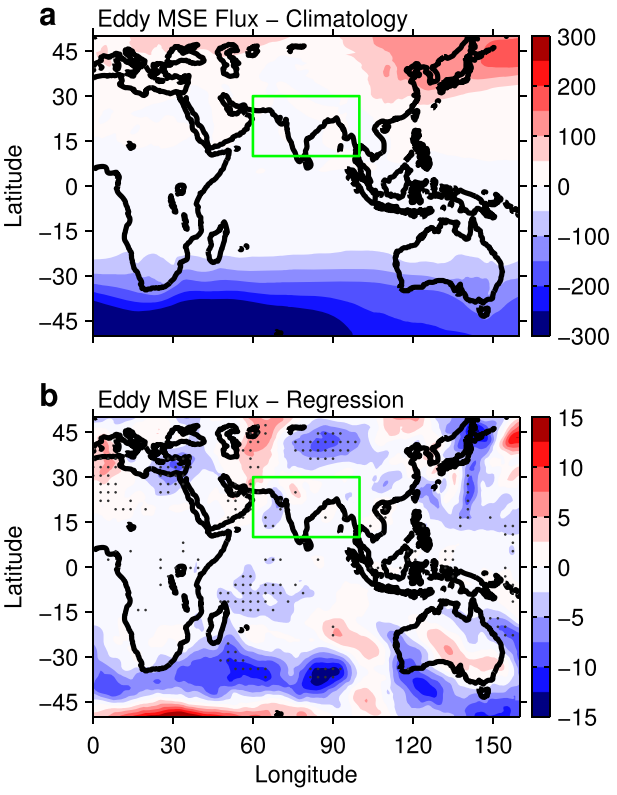

FIG. 11. (a) Climatology and (b) regression coefficient onto monsoon index of JJAS ERA-Interim vertically integrated MSE transient eddy fluxes (kW m^{-1}). Gray stippling in (b) shows the regions where the regression coefficient is significant at the 5% level. The green rectangle shows the averaging region for the MFC index.

energy transport away from, and a moisture transport toward, the differentially heated hemisphere. The findings that strong SASM years are associated with both a poleward shift of the circulation's ascending branch (Fig. 4) and anomalous cooling in the Southern Hemisphere midlatitudes (Fig. 9) suggest that similar mechanisms may be operating within the SASM sector on interannual time scales.

To investigate this further, we perform linear regression analysis of the mass-weighted vertically integrated transient eddy fluxes of moist static energy (MSE) against the MFC index. We find that strong monsoons are associated with negative anomalies in MSE eddy fluxes, dominated by dry static energy fluxes, in a wide band from approximately 30° to 45°S (Fig. 11). Although this feature is only statistically significant in a narrow range of longitudes according to the pointwise *t* test we use, it is spatially correlated across a broad longitude band, suggesting it is dynamically significant. It is also robust across all reanalysis datasets except NCEP2. This suggests that within the SASM sector during strong monsoons, extratropical cooling and increased poleward eddy energy flux in the Southern Hemisphere might play a role in the northward shift of the monsoon circulation, in analogy to the response of the zonally averaged precipitation to extratropical forcing. Lending further evidence to this hypothesis, we find that an increase of one standard deviation in MFC is associated with a statistically significant anomalous cross-equatorial MSE transport (primarily by the mean meridional overturning circulation) of −1.7 PW across the SASM sector; that is, the northward shift of the SASM circulation and anomalous cooling in the Southern Hemisphere extratropics during a strong monsoon are accompanied by anomalous southward cross-equatorial energy transport toward the differentially cooler hemisphere.[1] Of course, these correlations alone are not sufficient to establish causality, and future modeling work will be needed to determine the mechanisms involved and the direction of causality.

The Southern Hemisphere cooling associated with strong SASM is also consistent with findings by Wang et al. (2013) for the global monsoon, who found that there is a significant positive correlation between the strength of the Northern Hemisphere summer monsoon and the thermal contrast between the northern and southern hemispheres.

Since the eddy dry static energy fluxes comprise the vertical component of the Eliassen–Palm (EP) flux, our findings suggest that variations in Southern Hemisphere wave activity are associated with monsoon variations. To further explore this teleconnection, we look at the eddy momentum fluxes, which represent the meridional component of the EP flux. We perform linear regression analysis of the SASM sector eddy momentum flux divergence (EMFD) and zonal winds onto the MFC index. Figure 8a shows the JJAS climatology of the SASM sector zonal winds and transient EMFD. In the Southern Hemisphere, we see a region of momentum divergence in the upper troposphere extending approximately from 15°S to 30°S, within the subtropical westerly jet centered near 30°S, a region of momentum convergence in the upper troposphere extending approximately 30°–60°S, within the region of maximum baroclinicity, and a midlatitude jet centered near 45°S. The zero contour of the zonal wind closely follows the edge of the region of EMFD, indicating that large-scale extratropical eddies

[1] We find a similar result when using the energy fluxes from ERA-Interim derived components provided by NCAR (https://climatedataguide.ucar.edu/climate-data/era-interim-derived-components), in which the mass budget is balanced with a barotropic wind correction (Trenberth 1997b).

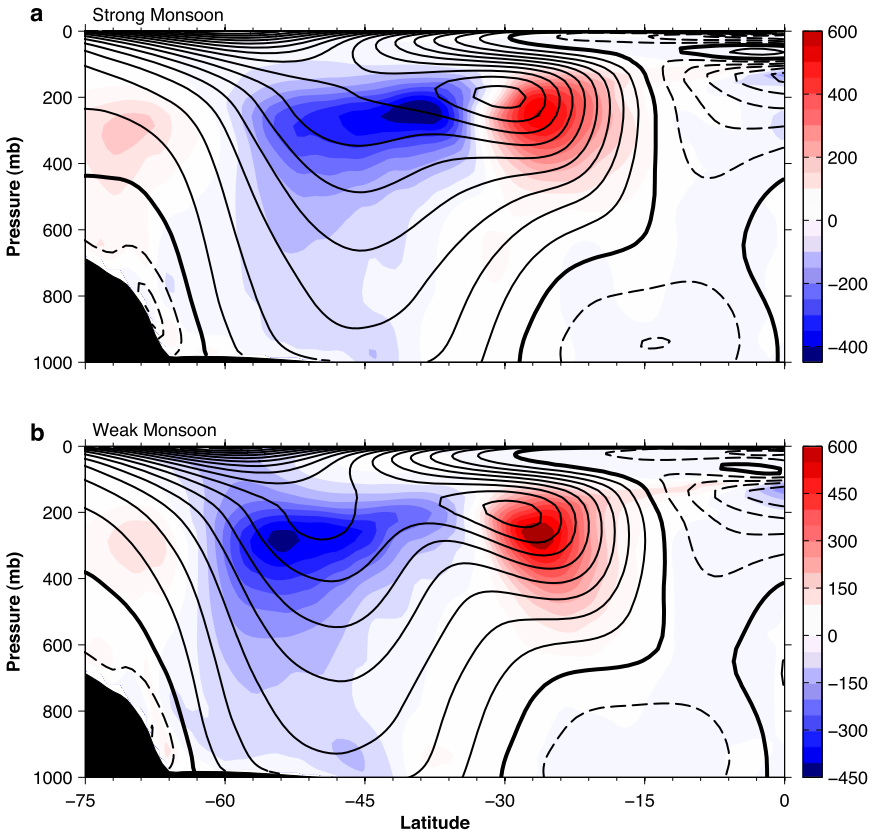

FIG. 12. Southern Hemisphere JJAS ERA-Interim SASM sector EMFD (colors, m s^{-2}) and zonal wind (contours, m s^{-1}) representing (a) strong and (b) weak SASM years. Zonal wind contours are 5 m s^{-1}, with positive contours solid, negative contours dashed, and zero contours thick solid. Black shading shows the sector mean topography.

do not propagate past their critical latitudes (Randel and Held 1991).

The linear regression of EMFD and zonal wind onto the MFC index reveals correlations in the Southern Hemisphere extratropics that are robust across datasets. Both regression fields display a dipole pattern, in which strong monsoons are associated with positive (negative) anomalies in zonal wind (EMFD) from approximately 20° to 45°S and negative (positive) anomalies in zonal wind (EMFD) from approximately 45° to 70°S (Fig. 8). Figure 12 shows strong and weak SASM composites (as defined in the previous section) of zonal wind and EMFD in the Southern Hemisphere. We can see that in strong monsoon years relative to weak monsoon years: 1) the midlatitude jet weakens and shifts approximately 3° equatorward (from ~49° to 46°S); 2) the subtropical jet strengthens and shifts approximately 2° poleward (from ~29° to 31°S); 3) the separation between the subtropical and midlatitude jets is reduced from approximately 20° to 15°; and 4) the region of eddy momentum flux convergence strengthens and its maximum shifts approximately 15° equatorward (from ~54° to 39°S). These features of strong SASM years suggest an equatorward shift of the midlatitude jet, which comes closer to merging with the subtropical jet. This is consistent with the enhanced near-surface meridional temperature gradient between the Southern Hemisphere subtropics and midlatitudes (Fig. 9d), implying stronger upper-level westerlies between 20° and 45°S, by thermal wind balance (Fig. 7d). These anomalies result in enhanced baroclinicity farther equatorward and so more eddy momentum flux convergence (wave activity divergence) farther equatorward. The strengthened subtropical jet may also result from increased angular momentum advection by the stronger monsoonal circulation.

The changes in Southern Hemisphere extratropical EMFD and eddy-driven jet that accompany strong (weak) monsoons are similar to those associated with southern annular mode variability (Thompson and Wallace 2000; Barnes and Hartmann 2010; Hendon et al. 2014), although more zonally localized. This suggests an association between SASM and southern annular mode variability, which will be explored in more depth in future work. These features are also qualitatively

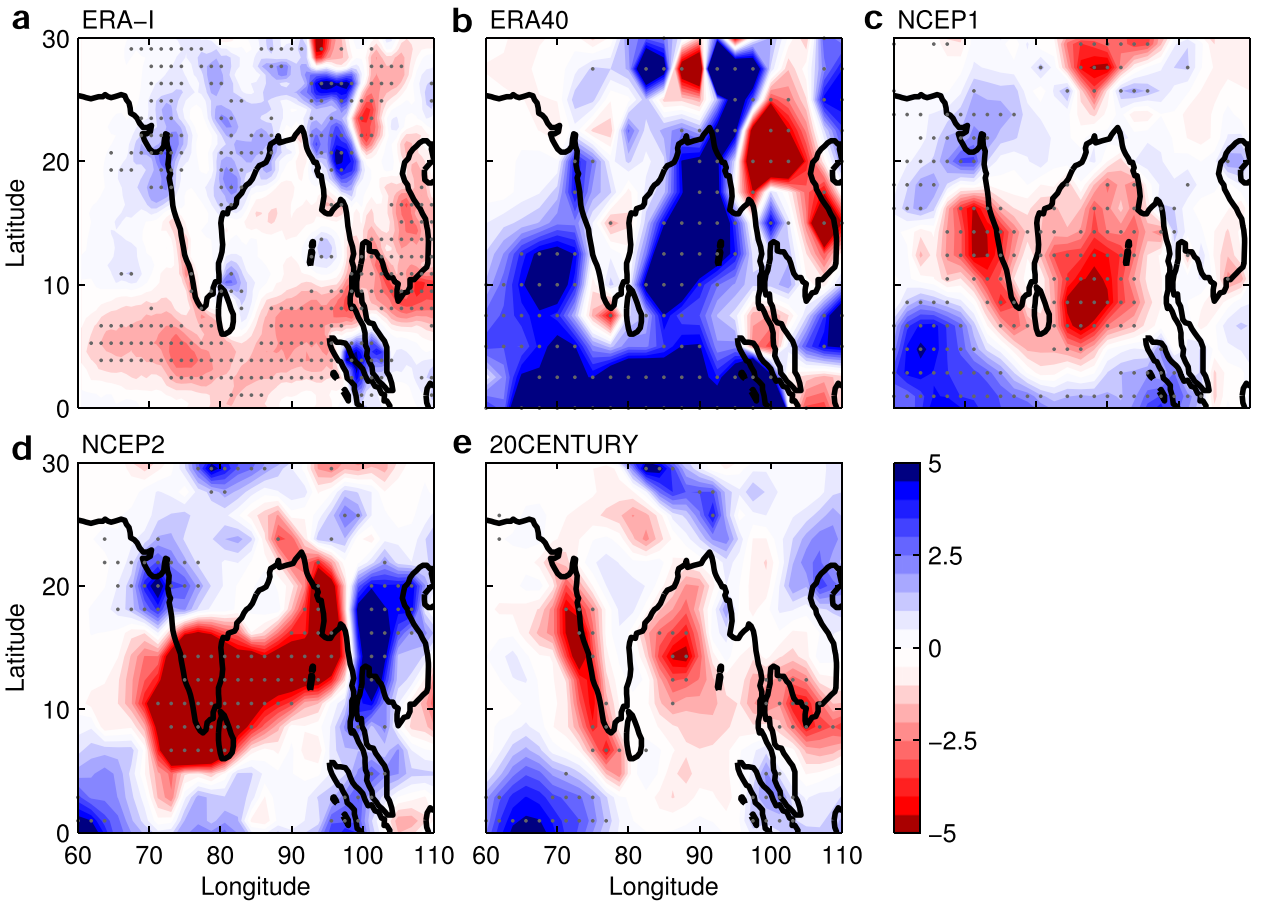

FIG. A1. Linear trend (mm day^{-1} yr^{-1}) in reanalysis precipitation over the period 1979–2011 (ERA-40: 1979–2002). Gray stippling shows the regions where the trend is significant at the 5% level.

consistent with findings by Ceppi and Hartmann (2013), who find interannual correlations between the position of the descending branch of the Hadley cell and the speed of the eddy-driven jet in the zonal mean.

6. Correlations with modes of SST variability

Since ENSO is one of the main modes of interannual variability associated with the SASM strength (e.g., Meehl 1987; Webster et al. 1998), we use the ENSO index described in section 2 to determine the correlation between the MFC index and ENSO, as well as the extent to which our findings are correlated with ENSO variability.

There is a statistically significant negative correlation of −0.39 between MFC and ENSO, consistent with previous studies, which have found that strong El Niño warm events are often associated with Indian monsoon failures (e.g., Pant and Parthasarathy 1981; Rasmusson and Carpenter 1982).

To investigate the role of ENSO variability in the findings presented in sections 4 and 5, we repeat the analyses with linear variability associated with the ENSO index removed from all fields and the resulting fields regressed onto the MFC index (not shown). We find that the anomalies in the monsoonal meridional overturning circulation, precipitation, and temperature within the SASM region and Southern Hemisphere EMFD in strong (weak) monsoons are not significantly related to ENSO variability. Some anomalies in extratropical zonal wind, temperature, and eddy energy fluxes associated with strong (weak) monsoons are partially related to, but not completely accounted for, by ENSO variability; these anomalies are weakened but still evident and statistically significant when ENSO variability is removed. In general, ENSO variability is not the predominant mode of variability for any of the findings presented here.

Since ENSO and IOD both measure zonal asymmetries of SSTs, we also use both indices to explore in more detail the anticorrelation in monsoon precipitation

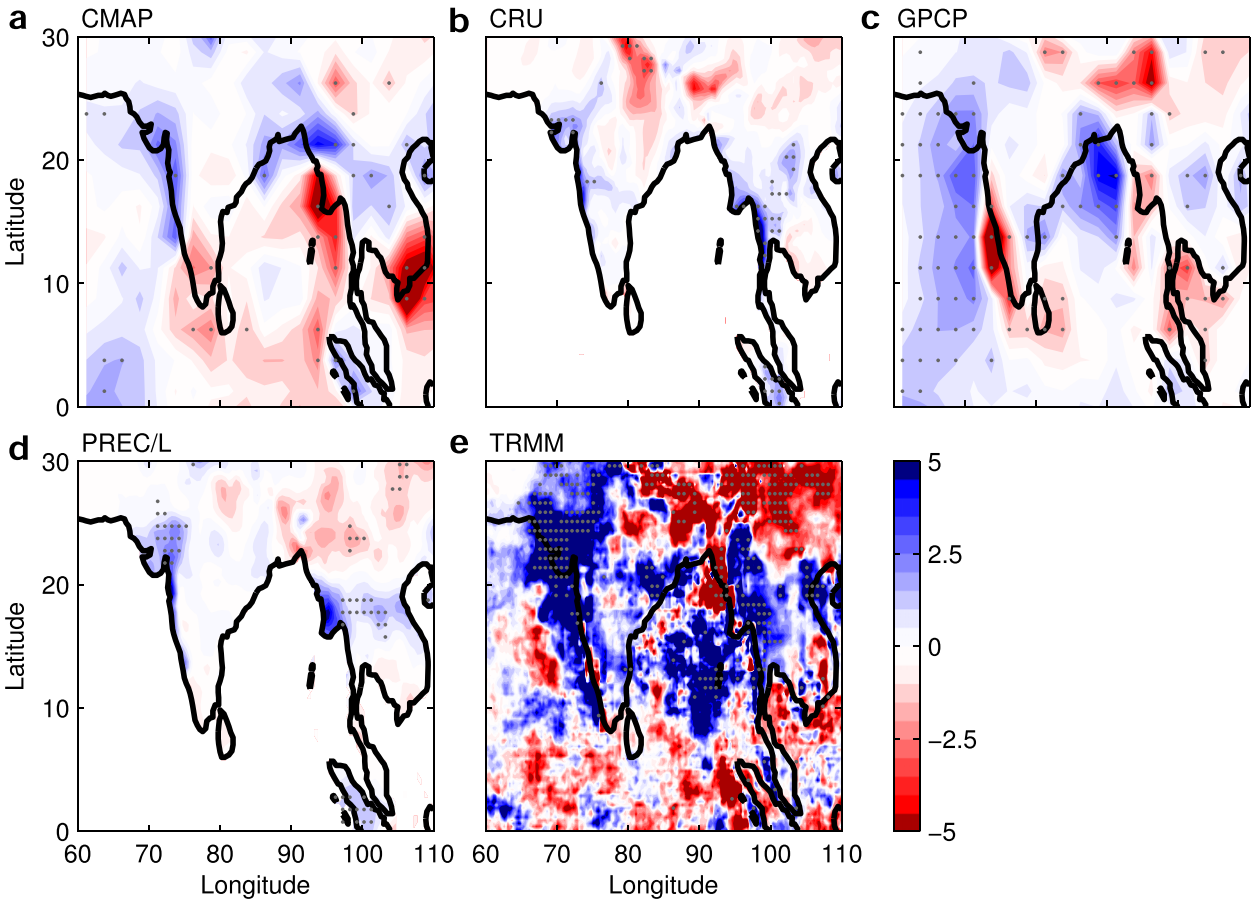

FIG. A2. As in Fig. A1, but for various other precipitation datasets. Trends computed over 1979–2011 (TRMM: 1998–2011).

anomalies between the eastern Bay of Bengal and the rest of the SASM domain (see Fig. 3 and the related discussion in section 4). We find that the anticorrelation is still evident and statistically significant when ENSO is removed. A similar analysis shows that the IOD index, described in section 2, also has a negligible contribution to the anticorrelation in the precipitation anomalies. Thus, the zonal asymmetry in interannual variability of precipitation between South Asia and the eastern Bay of Bengal is not linearly related to either ENSO or IOD.

7. Summary and concluding remarks

We investigated the interannual variability of precipitation and large-scale dynamics of the SASM using reanalysis and precipitation data from various sources. Using the vertically integrated moisture flux convergence in the SASM region as an index for monsoon strength, we decomposed the net precipitation variability into dynamic and thermodynamic components, and we performed linear regression analyses to identify numerous coherent and robust large-scale atmospheric patterns associated with monsoon variations. We find the following:

1) The interannual variability of SASM precipitation is mainly due to variability in circulation rather than variability in moisture.
2) Strong monsoons are characterized by a northward shift of the ascending branch of the cross-equatorial monsoonal circulation.
3) There is a negative correlation between the SASM strength and the near-surface thermal contrast between the continent and the Indian Ocean, in disagreement with the traditional view of monsoons as land–sea breeze circulations. This suggests that the near-surface atmospheric temperature distribution is itself a response to the atmospheric circulation rather than a forcing factor.
4) Within the SASM sector, teleconnections exist between the monsoon strength and the Southern Hemisphere extratropical atmospheric temperatures, eddy MSE fluxes, EMFD, and jet structure.

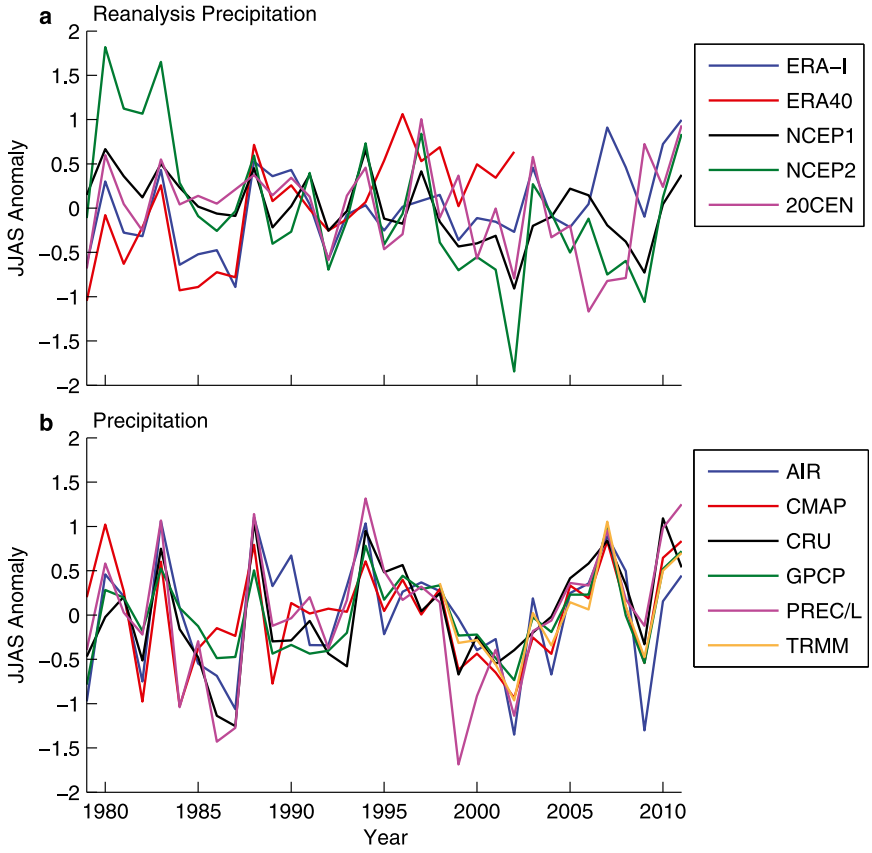

FIG. A3. Anomalies in SASM JJAS precipitation (mm day^{-1}) in reanalysis and precipitation data over the period 1979–2011 (ERA-40: 1979–2002 and TRMM: 1998–2011). All values are based on area averages over the region 10°–30°N, 60°–100°E, except AIR, which is an average over India.

In the Southern Hemisphere extratropics, strong SASM years are correlated with near-surface atmospheric cooling and increased poleward eddy fluxes of MSE in the Southern Hemisphere midlatitudes, suggesting that extratropical thermal forcing in the winter hemisphere may play a role in the northward shift of the monsoonal circulation during strong monsoons. Strong monsoons are also associated with Southern Hemisphere variability similar to the southern annular mode, with a northward shift and strengthening of eddy momentum flux convergence in the Southern Hemisphere extratropics, accompanied by a northward shift of the midlatitude westerly jet and strengthening of the subtropical westerly jet.

Although our findings are suggestive of a possible mechanism contributing to the interannual variability of the SASM (namely, an extratropical thermal forcing in the Southern Hemisphere leading to a northward shift in the monsoonal circulation during strong monsoons), in order to confirm causality the observational analysis will need to be supplemented with modeling work, including an analysis of zonal energy fluxes, to assess the extent to which mechanisms found in the zonal mean are operating within the SASM sector. Modeling studies similar to Kang et al. (2014) may be relevant to understanding the mechanisms underlying the observational findings presented here. In addition, although the northward shift of the monsoonal circulation during strong monsoons is a robust finding across all datasets examined here, these datasets are inconclusive regarding whether the northward shift in circulation is accompanied by a northward shift in the latitude of maximum precipitation within the SASM sector. Further analysis is needed to clarify this relationship. Despite these caveats, this study reveals robust large-scale connections between the Southern Hemisphere and the SASM on interannual time scales. Further examination of these connections will eventually result in better understanding and prediction of SASM interannual variability.

In contrast to the interannual variability we examined, changes in monsoon precipitation in response to greenhouse warming in climate models are dominated

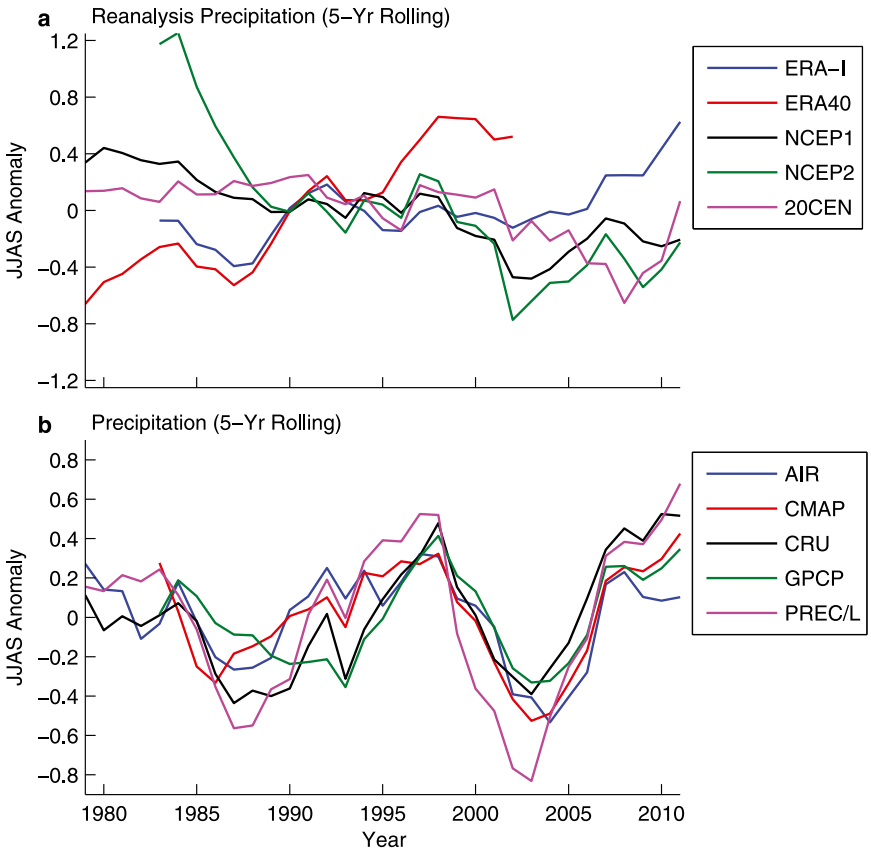

FIG. A4. As in Fig. A3, but with 5-yr running mean.

by the thermodynamic component, rather than the dynamic component (e.g., Cherchi et al. 2011; Hsu et al. 2013). Since these global warming simulations cover a much wider range of temperature increases than the interannual variability within the current climate, it seems reasonable that the thermodynamic component plays a much larger role in these climate experiments. It will be of interest to explore if SASM interannual variability in historical climate simulations in the World Climate Research Programme Coupled Model Intercomparison Project phase 5 (CMIP5) reveals similar patterns as the ones highlighted in this observational study.

Acknowledgments. This work was supported by a Natural Sciences and Engineering Research Council of Canada Postgraduate Scholarship, the Caltech Terrestrial Hazard Observation and Reporting Center, and National Science Foundation Grants AGS-1019211 and AGS-1049201. The data analyses were conducted on Caltech's Division of Geological and Planetary Science CITerra computing cluster.

APPENDIX

Long-Term Trends

In our analysis, we have focused on the interannual variability of the SASM during JJAS, with the long-term trends omitted from all fields. In this section we investigate long-term trends in SASM rainfall inferred from reanalysis, gauge-based, and satellite data products.

Identification of long-term trends in the seasonal-mean SASM rainfall is complicated by variability on interdecadal and subseasonal time scales, as well as regional variability within the SASM domain and inconsistencies between precipitation datasets. Some studies indicate the presence of a long-term decreasing trend in Indian summer monsoon rainfall since the mid-twentieth century (e.g., Ramanathan et al. 2005; Bollasina et al. 2011; Turner and Annamalai 2012). Gautam et al. (2009) find a steady increase in June rainfall over India in recent decades, accompanied by a decreasing trend in rainfall from July to September. Analysis of precipitation over numerous regions in India

TABLE A1. Linear trends in SASM JJAS yearly and 5-yr running mean precipitation [mm day^{-1} (33 yr)$^{-1}$] over the period 1979–2011 (ERA-40: 1979–2002 and TRMM: 1998–2011). All values are based on area averages over the region 10°–30°N, 60°–100°E, except AIR, which is an average over India. The trend in 5-yr running mean is omitted from TRMM due to insufficient number of years in the data. Trends that are statistically significant at the 5% level are in boldface.

Dataset	Yearly trend	5-yr trend
ERA-Interim	**+0.72**	**+0.59**
ERA-40	**+1.89**	**+1.87**
NCEP1	**−0.56**	**−0.72**
NCEP2	**−1.30**	**−1.56**
20CENTURY	−0.23	**−0.55**
AIR	+0.09	−0.10
CMAP	+0.12	+0.13
CRU	+0.68	+0.42
GPCP	+0.35	+0.23
PREC/L	+0.53	+0.12
TRMM	+1.95	N/A

indicates compensating positive and negative long-term trends in different regions, tending to cancel out in the area average (Naidu et al. 2009). Goswami et al. (2006) find increasing trends in the frequency and magnitude of extreme rain events over India in recent decades, with no significant long-term trend in the seasonal mean monsoon rainfall due to the compensating tendencies of extreme wet and dry events.

We investigate the long-term trends in SASM precipitation in the datasets previously discussed (ERA-Interim, ERA-40, NCEP1, NCEP2, 20CENTURY, GPCP, and AIR), as well as the following precipitation products: CPC Merged Analysis of Precipitation (CMAP), a merged analysis of rain gauge, satellite, and reanalysis data (Xie and Arkin 1997); gauge-based data from the University of East Anglia Climatic Research Unit (CRU; Harris et al. 2014); NOAA's gauge-based Precipitation Reconstruction over Land (PREC/L; Chen et al. 2002); and satellite-based precipitation estimates from NASA's Tropical Rainfall Measuring Mission (TRMM; Huffman et al. 2007). For all datasets we compute linear trends over the common period from 1979 to 2011, except for ERA-40 (1979–2002) and TRMM (1998–2011), which do not cover the entire 33-yr period.

Figures A1 and A2 show the linear trends in JJAS precipitation over the SASM domain. There is substantial regional variability throughout the domain, with most datasets indicating statistically significant positive and negative trends in different regions. There is little agreement between the datasets, and no robust regional patterns are evident.

The area average JJAS rainfall over the SASM domain is shown in Fig. A3 for the period 1979–2011, and the values filtered by a 5-yr running mean are shown in Fig. A4. In the unfiltered values in Fig. A3, it is evident that the interannual variability dominates over the long-term trend in all datasets except NCEP2. In the 5-yr running mean values (Fig. A4), we see positive trends in some datasets and negative trends in others, as well as strong interdecadal variability in all of the precipitation datasets (Fig. A4b), which is not evident in the reanalysis products (Fig. A4a). The linear trends computed from the SASM area averages are summarized in Table A1. Statistically significant trends are found only within the reanalysis products, and these include both positive and negative trends.

Thus, it is difficult to draw any general conclusions about the long-term trends in SASM rainfall in recent decades. Discrepancies among datasets are large, as are regional variations within the domain.

REFERENCES

Adler, R. F., and Coauthors, 2003: The Version-2 Global Precipitation Climatology Project (GPCP) monthly precipitation analysis (1979–present). *J. Hydrometeor.,* **4,** 1147–1167, doi:10.1175/1525-7541(2003)004<1147:TVGPCP>2.0.CO;2.

Ailikun, B., and T. Yasunari, 1998: On the two indices of Asian summer monsoon variability and their implications. *Extended Abstracts, Int. Conf. on Monsoon and Hydrologic Cycle,* Korean Meteorological Society, Kyongju, South Korea, 222–224.

Barnes, E. A., and D. L. Hartmann, 2010: Dynamical feedbacks of the southern annular mode in winter and summer. *J. Atmos. Sci.,* **67,** 2320–2330, doi:10.1175/2010JAS3385.1.

Bischoff, T., and T. Schneider, 2014: Energetic constraints on the position of the intertropical convergence zone. *J. Climate,* **27,** 4937–4951, doi:10.1175/JCLI-D-13-00650.1.

Blanford, H. F., 1884: On the connexion of the Himalaya snowfall with dry winds and seasons of drought in India. *Proc. Roy. Soc. London,* **37,** 3–22, doi:10.1098/rspl.1884.0003.

Bollasina, M. A., Y. Ming, and V. Ramaswamy, 2011: Anthropogenic aerosols and the weakening of the South Asian summer monsoon. *Science,* **334,** 502–505, doi:10.1126/science.1204994.

Bordoni, S., and T. Schneider, 2008: Monsoons as eddy-mediated regime transitions of the tropical overturning circulation. *Nat. Geosci.,* **1,** 515–519, doi:10.1038/ngeo248.

Broccoli, A. J., K. A. Dahl, and R. J. Stouffer, 2006: Response of the ITCZ to Northern Hemisphere cooling. *Geophys. Res. Lett.,* **33,** L01702, doi:10.1029/2005GL024546.

Ceppi, P., and D. L. Hartmann, 2013: On the speed of the eddy-driven jet and the width of the Hadley cell in the Southern Hemisphere. *J. Climate,* **26,** 3450–3465, doi:10.1175/JCLI-D-12-00414.1.

Chao, W. C., 2000: Multiple quasi equilibria of the ITCZ and the origin of monsoon onset. *J. Atmos. Sci.,* **57,** 641–652, doi:10.1175/1520-0469(2000)057<0641:MQEOTI>2.0.CO;2.

——, and B. Chen, 2001: The origin of monsoons. *J. Atmos. Sci.,* **58,** 3497–3507, doi:10.1175/1520-0469(2001)058<3497:TOOM>2.0.CO;2.

Chen, M., P. Xie, J. E. Janowiak, and P. A. Arkin, 2002: Global land precipitation: A 50-yr monthly analysis based on gauge observations. *J. Hydrometeor.,* **3,** 249–266, doi:10.1175/1525-7541(2002)003<0249:GLPAYM>2.0.CO;2.

Cherchi, A., and A. Navarra, 2013: Influence of ENSO and of the Indian Ocean dipole on the Indian summer monsoon variability. *Climate Dyn.,* **41,** 81–103, doi:10.1007/s00382-012-1602-y.

——, A. Alessandri, S. Masina, and A. Navarra, 2011: Effects of increased CO_2 levels on monsoons. *Climate Dyn.,* **37,** 83–101, doi:10.1007/s00382-010-0801-7.

Chiang, J. C. H., and C. M. Bitz, 2005: Influence of high latitude ice cover on the marine intertropical convergence zone. *Climate Dyn.,* **25,** 477–496, doi:10.1007/s00382-005-0040-5.

——, and A. R. Friedman, 2012: Extratropical cooling, interhemispheric thermal gradients, and tropical climate change. *Annu. Rev. Earth Planet. Sci.,* **40,** 383–412, doi:10.1146/annurev-earth-042711-105545.

Clement, A. C., A. Hall, and A. Broccoli, 2004: The importance of precessional signals in the tropical climate. *Climate Dyn.,* **22,** 327–341, doi:10.1007/s00382-003-0375-8.

Compo, G. P., and Coauthors, 2011: The Twentieth Century Reanalysis Project. *Quart. J. Roy. Meteor. Soc.,* **137,** 1–28, doi:10.1002/qj.776.

Dai, A., H. Li, Y. Sun, L.-C. Hong, LinHo, C. Chou, and T. Zhou, 2013: The relative roles of upper and lower tropospheric thermal contrasts and tropical influences in driving Asian summer monsoons. *J. Geophys. Res. Atmos.,* **118,** 7024–7045, doi:10.1002/jgrd.50565.

Dee, D. P., and Coauthors, 2011: The ERA-Interim reanalysis: Configuration and performance of the data assimilation system. *Quart. J. Roy. Meteor. Soc.,* **137,** 553–597, doi:10.1002/qj.828.

Emanuel, K. A., J. D. Neelin, and C. S. Bretherton, 1994: On large-scale circulations in convecting atmospheres. *Quart. J. Roy. Meteor. Soc.,* **120,** 1111–1143, doi:10.1002/qj.49712051902.

Frierson, D. M. W., and Y.-T. Hwang, 2012: Extratropical influence on ITCZ shifts in slab ocean simulations of global warming. *J. Climate,* **25,** 720–733, doi:10.1175/JCLI-D-11-00116.1.

Gadgil, S., 2003: The Indian monsoon and its variability. *Annu. Rev. Earth Planet. Sci.,* **31,** 429–467, doi:10.1146/annurev.earth.31.100901.141251.

——, and K. Kumar, 2006: The Asian monsoon—Agriculture and economy. *The Asian Monsoon,* B. Wang, Ed., Praxis Publishing, 651–683.

Gautam, R., N. C. Hsu, K.-M. Lau, and M. Kafatos, 2009: Aerosol and rainfall variability over the Indian monsoon region: Distributions, trends and coupling. *Ann. Geophys.,* **27,** 3691–3703, doi:10.5194/angeo-27-3691-2009.

Gill, A. E., 1980: Some simple solutions for heat-induced tropical circulation. *Quart. J. Roy. Meteor. Soc.,* **106,** 447–462, doi:10.1002/qj.49710644905.

Goswami, B. N., V. Krishnamurthy, and H. Annmalai, 1999: A broad-scale circulation index for the interannual variability of the Indian summer monsoon. *Quart. J. Roy. Meteor. Soc.,* **125,** 611–633, doi:10.1002/qj.49712555412.

——, V. Venugopal, D. Sengupta, M. S. Madhusoodanan, and P. K. Xavier, 2006: Increasing trend of extreme rain events over India in a warming environment. *Science,* **314,** 1442–1445, doi:10.1126/science.1132027.

Hahn, D. G., and J. Shukla, 1976: An apparent relationship between Eurasian snow cover and Indian monsoon rainfall. *J. Atmos. Sci.,* **33,** 2461–2462, doi:10.1175/1520-0469(1976)033<2461:AARBES>2.0.CO;2.

Harris, I., P. D. Jones, T. J. Osborn, and D. H. Lister, 2014: Updated high-resolution grids of monthly climatic observations—The CRU TS3.10 dataset. *Int. J. Climatol.,* **34,** 623–642, doi:10.1002/joc.3711.

Held, I. M., and B. J. Soden, 2006: Robust responses of the hydrological cycle to global warming. *J. Climate,* **19,** 5686–5699, doi:10.1175/JCLI3990.1.

Hendon, H. H., E.-P. Lim, and H. Nguyen, 2014: Seasonal variations of subtropical precipitation associated with the southern annular mode. *J. Climate,* **27,** 3446–3460, doi:10.1175/JCLI-D-13-00550.1.

Hsu, P.-C., T. Li, H. Murakami, and A. Kitoh, 2013: Future change of the global monsoon revealed from 19 CMIP5 models. *J. Geophys. Res. Atmos.,* **118,** 1247–1260, doi:10.1002/jgrd.50145.

Huffman, G. J., and Coauthors, 2007: The TRMM Multisatellite Precipitation Analysis (TMPA): Quasi-global, multiyear, combined-sensor precipitation estimates at fine scales. *J. Hydrometeor.,* **8,** 38–55, doi:10.1175/JHM560.1.

Hurley, J. V., and W. R. Boos, 2013: Interannual variability of monsoon precipitation and subcloud equivalent potential temperature. *J. Climate,* **26,** 9507–9527, doi:10.1175/JCLI-D-12-00229.1.

Kalnay, E., and Coauthors, 1996: The NCEP/NCAR 40-Year Reanalysis Project. *Bull. Amer. Meteor. Soc.,* **77,** 437–471, doi:10.1175/1520-0477(1996)077<0437:TNYRP>2.0.CO;2.

Kanamitsu, M., W. Ebisuzaki, J. Woollen, S.-K. Yang, J. J. Hnilo, M. Fiorino, and G. L. Potter, 2002: NCEP–DOE AMIP-II Reanalysis (R-2). *Bull. Amer. Meteor. Soc.,* **83,** 1631–1643, doi:10.1175/BAMS-83-11-1631.

Kang, S. M., I. M. Held, D. M. W. Frierson, and M. Zhao, 2008: The response of the ITCZ to extratropical thermal forcing: Idealized slab-ocean experiments with a GCM. *J. Climate,* **21,** 3521–3532, doi:10.1175/2007JCLI2146.1.

——, ——, and S.-P. Xie, 2014: Contrasting the tropical responses to zonally asymmetric extratropical and tropical thermal forcing. *Climate Dyn.,* **42,** 2033–2043, doi:10.1007/s00382-013-1863-0.

Kumar, K. K., B. Rajagopalan, and M. A. Cane, 1999: On the weakening relationship between the Indian monsoon and ENSO. *Science,* **284,** 2156–2159, doi:10.1126/science.284.5423.2156.

——, ——, M. Hoerling, G. Bates, and M. Cane, 2006: Unraveling the mystery of Indian monsoon failure during El Niño. *Science,* **314,** 115–119, doi:10.1126/science.1131152.

Li, C., and M. Yanai, 1996: The onset and interannual variability of the Asian summer monsoon in relation to land–sea thermal contrast. *J. Climate,* **9,** 358–375, doi:10.1175/1520-0442(1996)009<0358:TOAIVO>2.0.CO;2.

Lindzen, R. S., and A. Y. Hou, 1988: Hadley circulations for zonally averaged heating centered off the equator. *J. Atmos. Sci.,* **45,** 2416–2427, doi:10.1175/1520-0469(1988)045<2416:HCFZAH>2.0.CO;2.

Meehl, G. A., 1987: The annual cycle and interannual variability in the tropical Pacific and Indian Ocean regions. *Mon. Wea. Rev.,* **115,** 27–50, doi:10.1175/1520-0493(1987)115<0027:TACAIV>2.0.CO;2.

——, 1994: Influence of the land surface in the Asian summer monsoon: External conditions versus internal feedbacks. *J. Climate,* **7,** 1033–1049, doi:10.1175/1520-0442(1994)007<1033:IOTLSI>2.0.CO;2.

Merlis, T. M., T. Schneider, S. Bordoni, and I. Eisenman, 2013: The tropical precipitation response to orbital precession. *J. Climate,* **26,** 2010–2021, doi:10.1175/JCLI-D-12-00186.1.

Molnar, P., W. R. Boos, and D. S. Battisti, 2010: Orographic controls on climate and paleoclimate of Asia: Thermal and mechanical roles for the Tibetan Plateau. *Annu. Rev. Earth Planet. Sci.,* **38,** 77–102, doi:10.1146/annurev-earth-040809-152456.

Naidu, C. V., K. Durgalakshmi, K. Muni Krishna, S. Ramalingeswara Rao, G. C. Satyanarayana, P. Lakshminarayana, and L. Malleswara

Rao, 2009: Is summer monsoon rainfall decreasing over India in the global warming era? *J. Geophys. Res.,* **114,** D24108, doi:10.1029/2008JD011288.

Nie, J., W. R. Boos, and Z. Kuang, 2010: Observational evaluation of a convective quasi-equilibrium view of monsoons. *J. Climate,* **23,** 4416–4428, doi:10.1175/2010JCLI3505.1.

Pant, G. B., and S. B. Parthasarathy, 1981: Some aspects of an association between the Southern Oscillation and Indian summer monsoon. *Arch. Meteor. Geophys. Bioklimatol.,* **29B,** 245–252, doi:10.1007/BF02263246.

Parthasarathy, B., R. Kumar, and D. Kothawale, 1992: Indian summer monsoon rainfall indices, 1871–1990. *Meteor. Mag.,* **121,** 174–186.

——, A. Munot, and D. Kothawale, 1995: Monthly and seasonal rainfall series for all-India homogeneous regions and meteorological subdivisions: 1871–1994. Indian Institute of Tropical Meteorology Research Rep. RR-065, 113 pp.

Peixoto, J. P., and A. H. Oort, 1992: *Physics of Climate.* American Institute of Physics, 520 pp.

Privé, N. C., and R. A. Plumb, 2007: Monsoon dynamics with interactive forcing. Part I: Axisymmetric studies. *J. Atmos. Sci.,* **64,** 1417–1430, doi:10.1175/JAS3916.1.

Ramanathan, V., and Coauthors, 2005: Atmospheric brown clouds: Impacts on South Asian climate and hydrological cycle. *Proc. Natl. Acad. Sci. USA,* **102,** 5326–5333, doi:10.1073/pnas.0500656102.

Randel, W. J., and I. M. Held, 1991: Phase speed spectra of transient eddy fluxes and critical layer absorption. *J. Atmos. Sci.,* **48,** 688–697, doi:10.1175/1520-0469(1991)048<0688:PSSOTE>2.0.CO;2.

Rasmusson, E. M., and T. H. Carpenter, 1982: Variations in tropical sea surface temperature and surface wind fields associated with the Southern Oscillation/El Niño. *Mon. Wea. Rev.,* **110,** 354–384, doi:10.1175/1520-0493(1982)110<0354:VITSST>2.0.CO;2.

Saji, N. H., B. N. Goswami, P. N. Vinayachandran, and T. Yamagata, 1999: A dipole mode in the tropical Indian Ocean. *Nature,* **401,** 360–363.

Schneider, T., and S. Bordoni, 2008: Eddy-mediated regime transitions in the seasonal cycle of a Hadley circulation and implications for monsoon dynamics. *J. Atmos. Sci.,* **65,** 915–934, doi:10.1175/2007JAS2415.1.

——, T. Bischoff, and G. H. Haug, 2014: Migrations and dynamics of the intertropical convergence zone. *Nature,* **513**, 45–53, doi:10.1038/nature13636.

Shuen, X., M. Kimoto, and A. Sumi, 1998: Role of land surface processes associated with interannual variability of broad-scale Asian summer monsoon as simulated by the CCSR/NIES AGCM. *J. Meteor. Soc. Japan,* **76,** 217–236.

Shukla, J., and D. A. Mooley, 1987: Empirical prediction of the summer monsoon rainfall over India. *Mon. Wea. Rev.,* **115,** 695–704, doi:10.1175/1520-0493(1987)115<0695:EPOTSM>2.0.CO;2.

Simpson, G., 1921: The south-west monsoon. *Quart. J. Roy. Meteor. Soc.,* **199,** 150–173.

Sun, Y., Y. Ding, and A. Dai, 2010: Changing links between South Asian summer monsoon circulation and tropospheric land–sea thermal contrasts under a warming scenario. *Geophys. Res. Lett.,* **37,** L02704, doi:10.1029/2009GL041662.

Thompson, D. W. J., and J. M. Wallace, 2000: Annular modes in the extratropical circulation. Part I: Month-to-month variability. *J. Climate,* **13,** 1000–1016, doi:10.1175/1520-0442(2000)013<1000:AMITEC>2.0.CO;2.

Trenberth, K. E., 1997a: The definition of El Niño. *Bull. Amer. Meteor. Soc.,* **78,** 2771–2777, doi:10.1175/1520-0477(1997)078<2771:TDOENO>2.0.CO;2.

——, 1997b: Using atmospheric budgets as a constraint on surface fluxes. *J. Climate,* **10,** 2796–2809, doi:10.1175/1520-0442(1997)010<2796:UABAAC>2.0.CO;2.

——, J. Hurrell, and D. P. Stepaniak, 2005: The Asian monsoon: Global perspectives. *Asian Monsoon,* B. Wang, Ed., Praxis Publishing, 67–87.

Turner, A. G., and H. Annamalai, 2012: Climate change and the South Asian summer monsoon. *Nat. Climate Change,* **2,** 587–595, doi:10.1038/nclimate1495.

Uppala, S. M., and Coauthors, 2005: The ERA-40 Re-Analysis. *Quart. J. Roy. Meteor. Soc.,* **131,** 2961–3012, doi:10.1256/qj.04.176.

Wang, B., and Z. Fan, 1999: Choice of South Asian summer monsoon indices. *Bull. Amer. Meteor. Soc.,* **80,** 629–638, doi:10.1175/1520-0477(1999)080<0629:COSASM>2.0.CO;2.

——, R. Wu, and K.-M. Lau, 2001: Interannual variability of the Asian summer monsoon: Contrasts between the Indian and the western North Pacific–East Asian monsoons. *J. Climate,* **14,** 4073–4090, doi:10.1175/1520-0442(2001)014<4073:IVOTAS>2.0.CO;2.

——, J. Liu, H.-J. Kim, P. J. Webster, S.-Y. Yim, and B. Xiang, 2013: Northern Hemisphere summer monsoon intensified by mega-El Niño/Southern Oscillation and Atlantic multidecadal oscillation. *Proc. Natl. Acad. Sci. USA,* **110,** 5347–5352, doi:10.1073/pnas.1219405110.

Webster, P. J., 1972: Response of the tropical atmosphere to local, steady forcing. *Mon. Wea. Rev.,* **100,** 518–541, doi:10.1175/1520-0493(1972)100<0518:ROTTAT>2.3.CO;2.

——, and S. Yang, 1992: Monsoon and ENSO: Selectively interactive systems. *Quart. J. Roy. Meteor. Soc.,* **118,** 877–926, doi:10.1002/qj.49711850705.

——, and J. Fasullo, 2003: Monsoon—Dynamical theory. *Encyclopedia of Atmospheric Sciences,* J. R. Holton, Ed., Academic Press, 1370–1386.

——, V. O. Magaña, T. N. Palmer, J. Shukla, R. A. Tomas, M. Yanai, and T. Yasunari, 1998: Monsoons: Processes, predictability, and the prospects for prediction. *J. Geophys. Res.,* **103,** 14 451–14 510, doi:10.1029/97JC02719.

Wu, R., and B. P. Kirtman, 2003: On the impacts of the Indian summer monsoon on ENSO in a coupled GCM. *Quart. J. Roy. Meteor. Soc.,* **129,** 3439–3468, doi:10.1256/qj.02.214.

Xie, P., and P. A. Arkin, 1997: Global precipitation: A 17-year monthly analysis based on gauge observations, satellite estimates, and numerical model outputs. *Bull. Amer. Meteor. Soc.,* **78,** 2539–2558, doi:10.1175/1520-0477(1997)078<2539:GPAYMA>2.0.CO;2.

Yasunari, T., 1991: The monsoon year—A new concept of the climatic year in the tropics. *Bull. Amer. Meteor. Soc.,* **72,** 1331–1338, doi:10.1175/1520-0477(1991)072<1331:TMYNCO>2.0.CO;2.

Zuo, Z., S. Yang, R. Zhang, P. Jiang, L. Zhang, and F. Wang, 2013: Long-term variations of broad-scale Asian summer monsoon circulation and possible causes. *J. Climate,* **26,** 8947–8961, doi:10.1175/JCLI-D-12-00691.1.